Supplementary Information

Design of Potassiophilic 3D Conductive Scaffold Potassium Anode (3D-CTZ@K) with Dendrite-Free and High Energy-Power Density in Potassium Metal Batteries

Dong-Ting Zhang[a, b], Mao-Cheng Liu[a, b *], Min-Peng Li[a, b], Hao Chen[a, b], Chen-Yang Li[a, b], Yu-Xia Hu[a, b], Ling-Bin Kong[a, b], Xiang-Yun Zhang[a, b], Bing-Ni Gu[c, d, e, f], Ming-Jin Liu[c, d, e, f], Kun Zhao[a, b], Jun-Qiang Ren[a, b], Zi-Zhou Yuan[a, b *], Yu-Lun Chueh[c, d, e, f *]

[a]State Key Laboratory of Advanced Processing and Recycling of Non-ferrous Metals, Lanzhou University of Technology, Lanzhou 730050, People's Republic of China

[b]School of Materials Science and Engineering, Lanzhou University of Technology, Lanzhou 730050, People's Republic of China

[c]Department of Materials Science and Engineering, National Tsing Hua University, Hsinchu, 30013, Taiwan.

[d]Colleage of Semiconductor Research, National Tsing-Hua University, Hsinchu, 30013, Taiwan.

[e]Frontier Research Center on Fundamental and Applied Sciences of Matters, National Tsing Hua University, Hsinchu, 30013, Taiwan.

[f]Department of Physics, National Sun Yat-Sen University, Kaohsiung, 80424, Taiwan.

* E-mail: liumc@lut.edu.cn, yuanzz@lut.edu.cn, and ylchueh@mx.nthu.edu.tw

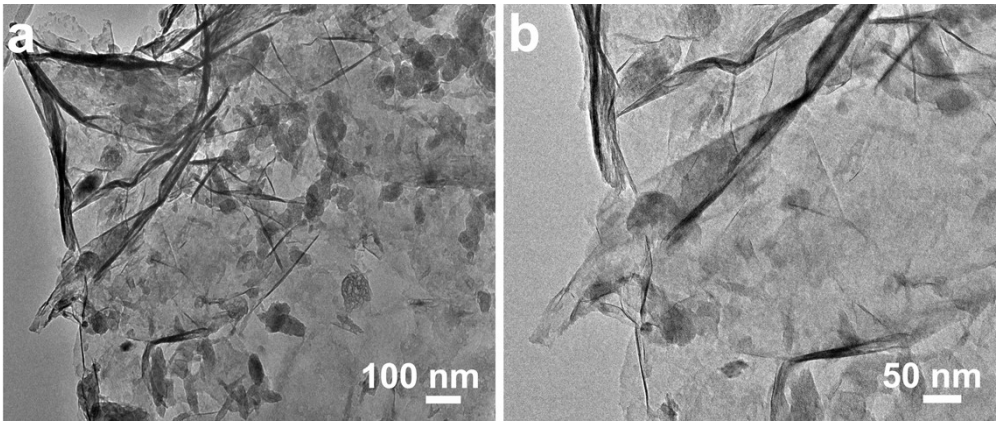

Figure S1 a, b) TEM images of TZ hybrids.

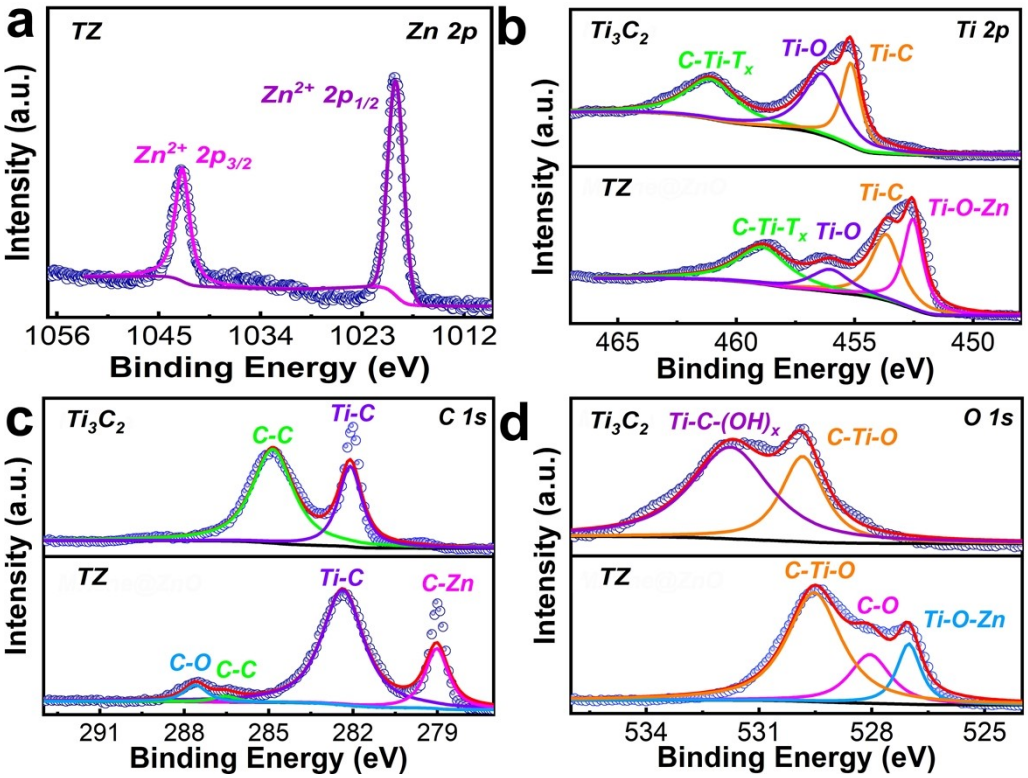

Figure S2 a) The high-resolution XPS spectra of Zn 2p in TZ hybrids. High-resolution XPS spectra of Ti_3C_2 and TZ hybrids, showing the fitting curves at b) Ti 2p, c) C 1s, and d) O 1s peaks, respectively.

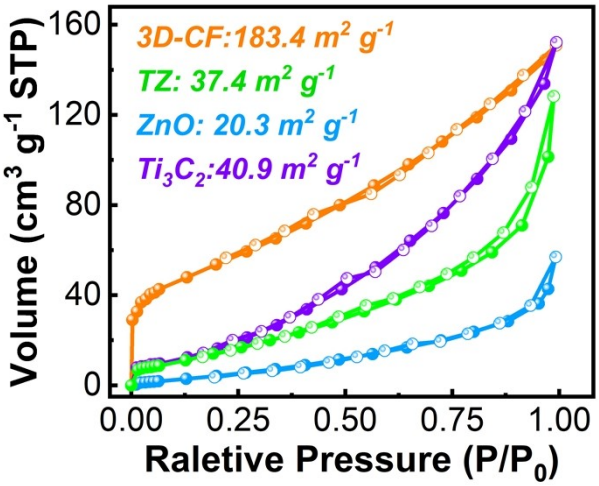

Figure S3 N_2 adsorption-desorption isotherm of 3D-CF, TZ, ZnO, and Ti_3C_2.

The SSA of 3D-CF, TZ, ZnO, and Ti_3C_2 are 183.4, 37.4, 20.3, and 40.9 m^2 g^{-1}, respectively. Compared with 3D-CF, the decreased SSA of 3D-CTZ is ascribed to the adhered of TZ hybrids, which take up some of the empty space in the 3D-CF.

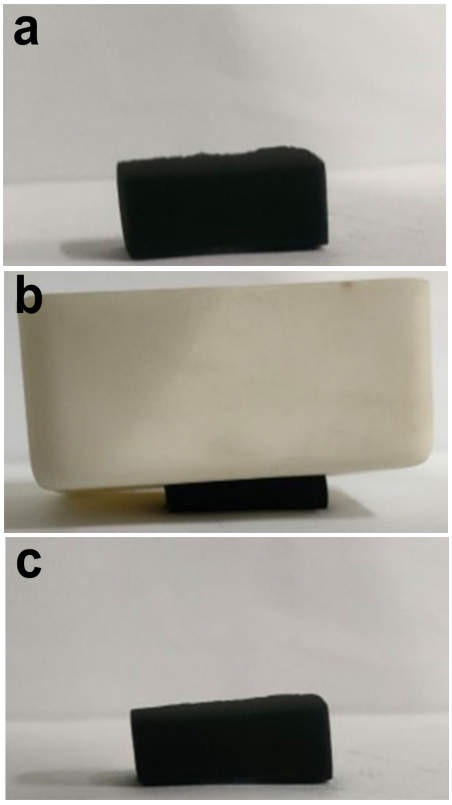

Figure S4 The macroscopic digital photo of 3D-CTZ scaffold (a) without the stress, (b) under the compressive stress, and (c) after removing the compressive stress.

It can be observed in the macroscopic digital photos that the 3D-CTZ scaffold undergoes deformation under pressure, and then recovers deformation and maintains the same after removing the compressive stress. The result proved that 3D-CTZ scaffold possesses the outstanding mechanical property, which is favorable to support the infusion of the molten K metal and buffer huge stress-strain during the K plating/stripping processes.

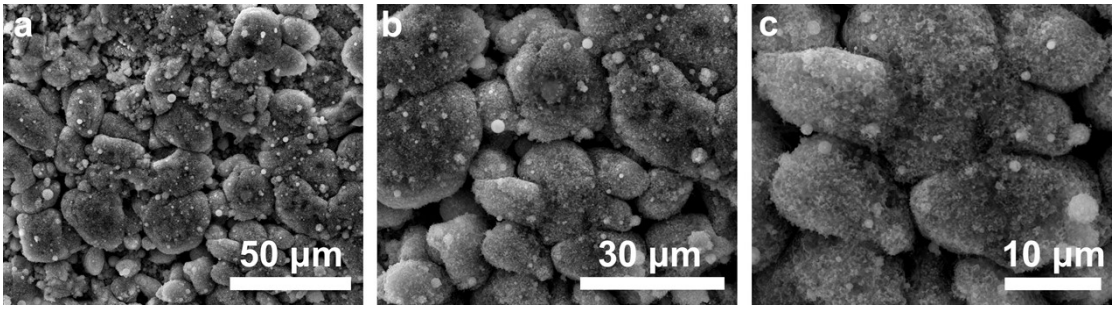

Figure S5 (a-c) Top-view SEM images of 3D-CTZ@K after 200 th cycles at the current density of 0.5 mA cm^{-2} and the cycling capacity of 0.5 mAh cm^{-2}.

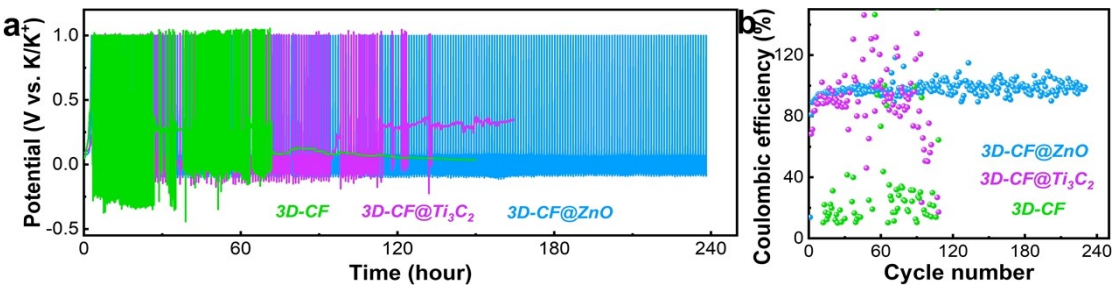

Figure S6 Electrochemical performance of K//3D-CF, K//3D-CF@Ti_3C_2, and K//3D-CF@ZnO half batteries. (a) Galvanostatic plating and stripping profiles for half-batteries at the current density of 1.0 mA cm^{-2}. (b) Coulombic efficiency.

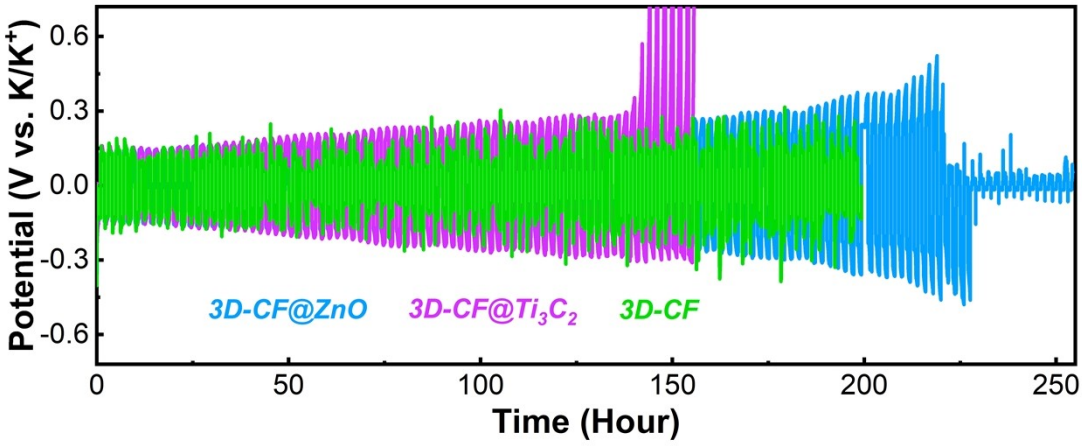

Figure S7 Galvanostatic cycle of 3D-CF@ZnO@K//3D-CF@ZnO@K, 3D-CF@Ti_3C_2@K//3D-CF@Ti_3C_2@K, and 3D-CF@K//3D-CF@K symmetrical batteries at the current density of 0.5 mA cm^{-2} with the capacity of 0.5 mAh cm^{-2} per cycle.

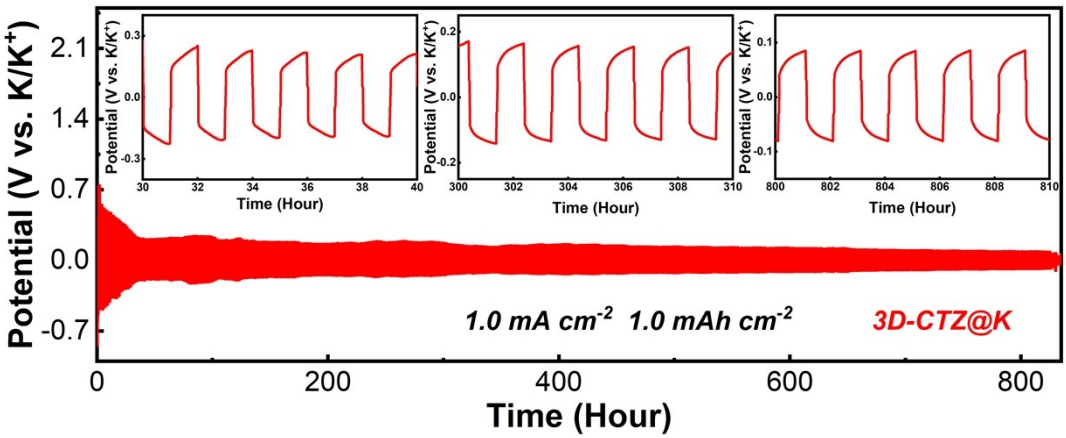

Figure S8. Galvanostatic cycles of 3D-CTZ@K//3D-CTZ@K batteries. The current density was fixed at 1.0 mA cm^{-2} with the capacity of 1.0 mAh cm^{-2} per cycle.

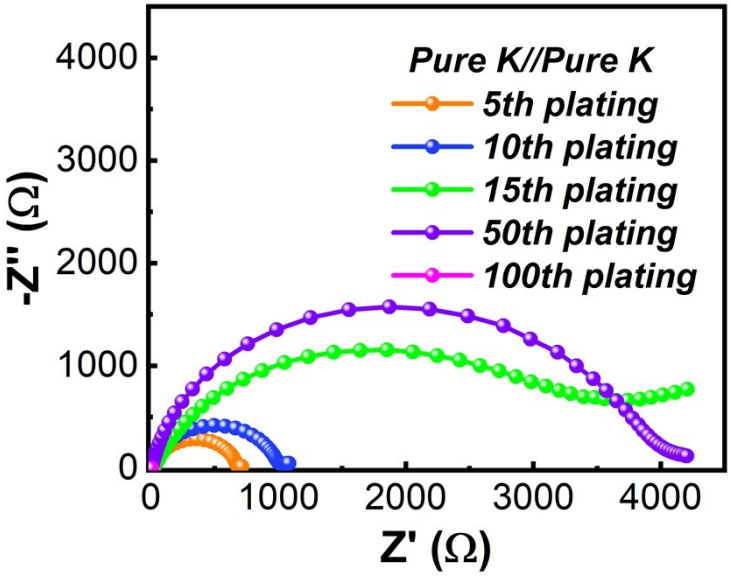

Figure S9. Nyquist plots of K//K battery after different cycles at 1.0 mA cm^{-2} to 1.0 mAh cm^{-2} per cycle.